Int. J. Radiation Oncology Biol. Phys., Vol. 60, No. 2, pp. 636–647, 2004

0360-3016/04/$–see front matter

ELSEVIER

doi:10.1016/j.ijrobp.2004.05.068

PHYSICS CONTRIBUTION

MRI-BASED TREATMENT PLANNING FOR RADIOTHERAPY: DOSIMETRIC VERIFICATION FOR PROSTATE IMRT

LILI CHEN, PH.D., ROBERT A. PRICE, JR., PH.D., LU WANG, PH.D., JINSHENG LI, PH.D., LIHONG QIN, PH.D., SHAWN MCNEELEY, M.S., C-M CHARLIE MA, PH.D., GARY M. FREEDMAN, M.D., AND ALAN POLLACK, PH.D., M.D.

Department of Radiation Oncology, Fox Chase Cancer Center, Philadelphia, PA

Purpose: **Magnetic resonance (MR) and computed tomography (CT) image fusion with CT-based dose calculation is the gold standard for prostate treatment planning. MR and CT fusion with CT-based dose calculation has become a routine procedure for intensity-modulated radiation therapy (IMRT) treatment planning at Fox Chase Cancer Center. The use of MRI alone for treatment planning (or MRI simulation) will remove any errors associated with image fusion. Furthermore, it will reduce treatment cost by avoiding redundant CT scans and save patient, staff, and machine time. The purpose of this study is to investigate the dosimetric accuracy of MRI-based treatment planning for prostate IMRT.**

Methods and Materials: **A total of 30 IMRT plans for 15 patients were generated using both MRI and CT data. The MRI distortion was corrected using gradient distortion correction (GDC) software provided by the vendor (Philips Medical System, Cleveland, OH). The same internal contours were used for the paired plans. The external contours were drawn separately between CT-based and MR imaging–based plans to evaluate the effect of any residual distortions on dosimetric accuracy. The same energy, beam angles, dose constrains, and optimization parameters were used for dose calculations for each paired plans using a treatment optimization system. The resulting plans were compared in terms of isodose distributions and dose–volume histograms (DVHs). Hybrid phantom plans were generated for both the CT-based plans and the MR-based plans using the same leaf sequences and associated monitor units (MU). The physical phantom was then irradiated using the same leaf sequences to verify the dosimetry accuracy of the treatment plans.**

Results: **Our results show that dose distributions between CT-based and MRI-based plans were equally acceptable based on our clinical criteria. The absolute dose agreement for the planning target volume was within 2% between CT-based and MR-based plans and 3% between measured dose and dose predicted by the planning system in the physical phantom.**

Conclusions: **Magnetic resonnace imaging is a useful tool for radiotherapy simulation. Compared with CT-based treatment planning, MR imaging–based treatment planning meets the accuracy for dose calculation and provides consistent treatment plans for prostate IMRT. Because MR imaging–based digitally reconstructed radiographs do not provide adequate bony structure information, a technique is suggested for producing a wire-frame image that is intended to replace the traditional digitally reconstructed radiographs that are made from CT information.** **© 2004 Elsevier Inc.**

Radiotherapy, MRI treatment planning, Prostate cancer, Dosimetry, IMRT.

INTRODUCTION

Prostate carcinoma is the most common malignancy in North American males and the second leading cause of cancer death. Disease confined to the prostate glad can be definitively treated with radical radiation therapy. However, in patients not achieving complete viable tumor clearance, a continued toll of local failure is observed (1). Recent investigations suggest that dose escalation with intensity-modulated radiation therapy (IMRT) potentially increases the local control while greatly reducing rectal and bladder exposure to high radiation doses (2–8). As dose levels are increased, the use of new imaging methods to more accurately target the prostate and the accuracy of dose delivery

Reprint requests to: Lili Chen, Ph.D., Radiation Oncology Department, Fox Chase Cancer Center, 333 Cottman Avenue, Philadelphia, PA 19111; Tel: (215) 728-3003; Fax: (215) 728-4789; E-mail: l_Chen@fccc.edu

The materials in this article have been partially presented at the ASTRO 2003 Annual Meeting in Salt Lake City.

Partially supported by grants from the NIH (CA78331) and DOD (PC030800).

Acknowledgments—We would like to thank Elizabeth A. Palacio and Teresa Richardson for help with MR scanning and Geraldine M. Shammo and Kevin L. Crawford for help with contouring and treatment planning. We would also like to thank the support from Philips Medical Systems, especially Dr. Michael Steckner and David Abraham for their excellent technical assistance.

Received Feb 24, 2004, and received in revised form May 26, 2004. Accepted for publication May 28, 2004.

become crucial. Magnetic resonance imaging (MRI) provides superior image quality for soft-tissue delineation over computed tomography (CT) and is widely used for target and organ delineation in radiotherapy for treatment planning (9–11). The prostate volume on CT appears much larger than on MRI (12). These results were consistent with those reported by Krempien *et al.* (13). Debois *et al.* (14) showed that improved prostate and rectal volume delineation from MRI could lead to improvements in both target coverage and rectal sparing. As a result of its improved soft-tissue delineation, using MRI for radiotherapy planning of prostate cancer is desirable. Although MRI-CT image fusion has been widely accepted as a practical approach for both accurate anatomic delineation (using MRI data) and dose calculation (using CT data), it would be ideal if MRI could be used alone for prostate treatment planning. The fusion process introduces additional error because it is often difficult to coordinate CT and magnetic resonance images, and differences in bladder and rectal filling may lead to substantial discordance. Furthermore, MRI-based treatment planning will avoid redundant CT imaging sessions, leading to reduced treatment cost and less radiation exposure to the patient.

More recently, studies have been carried out to explore the efficacy of MRI-based treatment planning for radiotherapy (15–22). However, the perceived disadvantages of using MRI for radiotherapy planning have precluded its widespread use in this area. These disadvantages include the lack of electron density information and image distortion leading to geometrical inaccuracies. MRI and CT image fusion with CT-based dose calculation is the gold standard for prostate treatment planning.

It has been generally accepted that there is no clinically significant difference in dose calculation between homogeneous and heterogeneous geometry assumptions for pelvic treatments. It has been common practice to use homogeneous geometry in treatment planning dose calculations for prostate cancer. This was also confirmed by Monte Carlo calculations for both conventional treatment and IMRT (23–25). Therefore, the lack of electron density information from MRI is not considered to be a significant problem in the context of treatment planning for prostate cancers.

Magnetic resonance imaging distortions affect the accuracy of dose calculation. It is clear that before MRI alone can be used for treatment planning for prostate patients, any image distortion must be quantified and corrected. Image distortion arises from both system-related effects and object-induced effects. System-related distortion is a result of inhomogeneities in the main magnetic and gradient fields, whereas object-induced effects are the result of both chemical shift and susceptibility effects because of the difference of the resonance between fat and water and the difference at tissue-air interfaces. For fields below about 0.5 T, imaging sequences that provide a sufficient signal-to-noise ratio maintain geometric distortion resulting from either of these object-related effects below 1–2 pixels. This is achieved by defining a lower limit for the bandwidth of the readout gradient during image acquisition (26). In our clinical MRI simulation routine, we have chosen 154 Hz/pixel in the frequency encoding direction; therefore, the effects caused by chemical and susceptibility are considered negligible. For system-related distortions, we have used gradient distortion correction (GDC) software to correct the MRI distortion. The GDC software was provided by the vendor (Philips Medical Systems, Cleveland, OH) and approved by the U.S. Food and Drug Administration. In this study, we explored the use of MRI-based treatment planning for prostate IMRT using the Corvus inverse planning system (NOMOS Corp., Sewickley, PA).

METHODS AND MATERIALS

The MRI scanner

A 0.23-Tesla open MRI scanner (Philips Medical Systems, Cleveland, OH) was used for this study. The MRI scanner consists of two poles approximately 1 m in diameter each. The separation between the two poles is 47 cm. The MRI scan table can be moved in orthogonal planes along a set of rails mounted on the floor and on an orthogonal set of rails built in the couch. Vertical adjustment can be accomplished using a composite flat top with hard foam spacers beneath the patient. A set of three triangulation lasers (center and laterals) identical to those used on linear accelerators has been used for patient positioning.

CT and MR imaging procedure

Patients were scanned on a CT simulator (PICKER PQ 5000, Philips Medical Systems, Cleveland, OH) with a field of view (FOV) of 480 mm, 512 × 512 matrix (spatial resolution 0.94 mm), and a slice thickness of 3 mm. The axial CT slices extended from the third lumbar vertebrae to the middle of the femurs. Patients were advised to have a full bladder and were scanned in a supine position in a customized alpha cradle with knee support and a foot holder. Three steel ball fiducials (1 mm in diameter) were used (one anterior and two laterals) on the skin surface to mark the center of the prostate as an isocentric slice. Skin tattoos corresponding to these fiducial markers were aligned for daily treatment set up. The CT data were transferred to the treatment planning workstation and the patient was transferred to the MRI room for scanning usually within 0.5 h after CT.

Patients were MRI-scanned in a supine position in an alpha cradle with knee support and a foot holder (the same as for CT). Three donut-shaped fiducials (IZI Medical Products, Inc., Baltimore, MD) were superimposed on the tattoos that mark the center of the prostate as indicated by CT. In this position, MRI landmarks were made. One axial reference image was obtained. A sagittal image was obtained through the center of the prostate as depicted on the axial image. A series of 48 axial slices covering the whole pelvis based on the sagittal image was acquired. The T2-weighted turbo spin echo, three-dimensional sequence was performed for this study. Detailed parameters are repetitive time/echo time (TR/TE) = 3000/140 ms, FOV = 450–500 cm (de-

pending on patients' anatomic dimensions), matrix = 256 × 256 (spatial resolution 1.76–1.95 mm), echo train length (ETL) = 32, Flip angle = 90°, slice thickness = 3 mm, number of excitations (NEX) = 1, bandwidth (BW) = 39.5 kHz with horizontal frequency direction, and 9-min scan time. The magnetic resonance images were postprocessed for image distortion correction using the GDC software. The distortion-corrected MRIs were transferred to the treatment planning workstation.

Target and structure delineation

In our institution, CT-MRI fusion with CT-based dose calculation has been a routine procedure for all prostate cancer patients. Each patient underwent a CT and MRI scan as part of a routine simulation procedure. CT and MRIs (after GDC) were fused according to bony anatomy using either chamfer matching or maximization of mutual information methods. These fusion methods are available in the AcQSim system (Philips Medical Systems) used for this work. After image fusion, an evaluation of the fusion was performed. The results were checked by contouring bony landmarks on a minimum of three different slices: the central slice of the prostate and a few slices superior and inferior to the central slice. Our criterion for acceptance of the fusion was that the contours of the bones matched to within 2 mm on all three slices. Fifteen patients' CT and MRI data were used for this study.

In our clinical routine fusion procedure, the CT images were loaded first as the primary image and the MRIs were loaded as the secondary image. The external contour was obtained using an automatic threshold program and the femoral heads were manually contoured based on the CT image. The targets and critical structures were delineated based on the MRIs by oncologists. All the contours either based on primary CT or on secondary MRI were saved on the primary CT data set and were used for CT-based treatment planning. For MRI-based treatment planning, we loaded the MRIs as the primary image and the CT as the secondary image. The external contours were generated directly on the MRI data. The same internal contours as used in CT-based treatment planning were used for MRI-based treatment planning by manually copying target and critical structure contours from CT to MRI according to the color wash images of these structures. This is a feature available on the AcQSim system when a previous primary image is reloaded as a secondary image (direct contour transfer from a primary image to a secondary image is not possible). Although manually transferring internal contours could introduce some small errors, it was considered to be more reliable to use the same internal structure contours for our plan comparison than using new contours generated independently on MRI because this would introduce additional and potentially more significant uncertainties in the contours between MRI-based and CT-based treatment planning.

Table 1. Patient lateral dimensions measured on CT (distortion-free) and the residual distortions on MRI calculated as the difference between external contour points along the lateral axis on the isocentric slice on CT and those on GDC-corrected MRI

No. of patients	Patient sizes (cm)	Maximum residual distortion (cm)
2	<36.0	0.2 (0.0–0.2)
5	36.0–38.0	0.7 (0.0–0.7)
4	38.5–40.0	1.0 (0.2–1.0)
4	>40.0	2.7 (0.3–2.7)

Abbreviations: CT = computed tomography; MRI = magnetic resonance imaging; GDC = gradient distortion correction.

Dose calculation and plan comparison

All the CT-based treatment plans were approved by oncologists according to our clinical criteria (see the following section) and were subsequently used for the treatment. The MRI-based IMRT plans were generated, only for plan comparison, using the same planning parameters as for CT-based planning in terms of the prescribed dose, fractions, beam energy, beam angles, dose constraints, and optimization parameters. We used 6-, 10-, and 18-MV photon beams and six to nine gantry angles/ports depending on patient's body geometry.

Paired plans were compared based on our clinical acceptance criteria for prostate IMRT at Fox Chase Cancer Center. The maximum dose must be lower than 120% of the prescribed dose. The 95% of the planning target volume (PTV) must receive ≥100% of the prescribed dose (D95). The volume of rectum receiving 40 Gy (V40) and 65 Gy (V65) must be ≤35% and ≤17%, respectively. For bladder, no well-defined criteria have been identified. As a consequence, we have initiated soft constraints such that V40 and V65 must be ≤50% and ≤25%, respectively. These constraints serve as a guide for treatment planning. There were many plans that did not meet the constraints because the bladder was not sufficiently full during simulation. For femoral heads, less than 10% of the volume (V10) should receive 50 Gy. The isodose distributions were examined on a slice-by-slice basis. Our acceptable range was that the minimum distance from the posterior edge of the prostate clinical target volume (CTV) to the prescription isodose line was 4 mm to 8 mm. No more than one slice was allowed to be <4 mm. The PTV is 8 mm larger than the CTV in all other directions. Additionally, the 90% isodose line must not encompass the half width of the rectum or the 50% isodose line must not encompass the full width of the rectum on any slice except in some cases in which the rectal volume was very small (27).

RESULTS

Measurement of target and structure volumes on CT and MRI

After a patient was scanned with MRI, the images were processed using the vendor provided GDC software. The

Table 2. Structure volumes (in cm^3) measured on MRI and on CT as reported by the Corvus system

Patient no.	GTV		SV		Rectum		Bladder	
	MRI	CT	MRI	CT	MRI	CT	MRI	CT
1	34	33	6	5	94	91	93	91
2	35	33	NA	NA	79	76	124	122
3	62	60	NA	NA	48	46	124	122
4	57	55	11	11	70	68	78	76
5	93	92	15	16	118	116	64	63
6	135	132	5	6	95	92	116	113
7	68	66	5	5	55	51	168	165
8	64	63	8	8	42	44	195	192
9	55	54	4	4	55	53	274	269
10	47	45	10	10	51	49	209	208
11	31	31	6	6	38	37	56	57
12	30	29	3	3	63	61	164	162
13	36	36	5	5	55	52	168	166
14	60	60	12	12	50	49	87	88
15	67	66	9	9	51	49	103	102

Abbreviations: MRI = magnetic resonance imaging; CT = computed tomography; GTV = gross tumor volume; SV = seminal vesicle.

MRI distortion was reduced significantly after the GDC. Table 1 summarizes the relationship between patient's anatomic size and the residual distortion error after GDC along the lateral axis on the isocenter slice. The residual error was within 1 cm for patients with lateral dimensions <40 cm.

An additional uncertainty in the dose–volume histogram (DVH) comparison (see the following section) between CT- and MRI-based treatment planning is the difference in the target and structure contours resulting from manual transfer from the CT data sets to the MRI data sets. Table 2 shows the values of the structure volumes measured on MRI and on CT on the Corvus system. The volumes of the GTV from MRI are consistently slightly greater than those measured from CT. The maximum differences of the GTV between the two data sets are 6% (2 cc in absolute volume), 20% (1 cc in absolute volume) on seminal vesicles (SVs) (range, 17–20%), 8% (4 cc in absolute volume) on rectums (range, 2–8%), and 3% (2 to 3 cc in absolute volume) on bladders (range, 0.5–3%). Small changes in contour volumes were also observed between the CT and MR images after they were transferred from the AcQSim system to the Corvus system. The volumes measured on Corvus were smaller than those from the AcQSim by up to 6%. Table 3 compares the ratios of the MRI volumes with the CT volumes between AcQSim and Corvus.

These small volume discrepancies between the two data sets were thought to be due to the image resolution and algorithmic differences in volume determination in the AcQSim software and the Corvus system, and to the uncertainties introduced by the manual transfer of the contours between the two data sets.

Table 3. Ratios of structure volumes shown on MRI and those shown on CT as reported by AcQSim and Corvus

Patient no.	GTV		SV		Rectum		Bladder	
	AcQSim	Corvus	AcQSim	Corvus	AcQSim	Corvus	AcQSim	Corvus
1	1.07	1.03	1.07	1.20	1.08	1.03	1.04	1.02
2	1.06	1.06	N/A	N/A	1.07	1.04	1.05	1.02
3	1.04	1.03	N/A	N/A	1.03	1.04	1.03	1.02
4	1.05	1.04	1.06	1.0	1.04	1.03	1.04	1.03
5	1.04	1.01	1.04	0.94	1.05	1.02	1.05	1.02
6	1.04	1.02	1.03	0.83	1.05	1.03	1.05	1.03
7	1.05	1.03	1.07	1.00	1.04	1.08	1.04	1.02
8	1.04	1.02	1.06	1.00	1.03	0.95	1.03	1.02
9	1.05	1.02	1.02	1.00	1.03	1.04	1.03	1.02
10	1.05	1.04	1.05	1.00	1.03	1.04	1.03	1.00
11	1.06	1.00	1.03	1.00	1.05	1.03	1.05	0.98
12	1.05	1.03	1.00	1.00	1.05	1.03	1.02	1.01
13	1.04	1.00	1.02	1.00	1.08	1.06	1.03	1.01
14	1.03	1.00	1.05	1.00	1.08	1.02	1.02	0.99
15	1.04	1.02	1.05	1.00	1.08	1.04	1.03	1.01

Abbreviations as in Table 2.

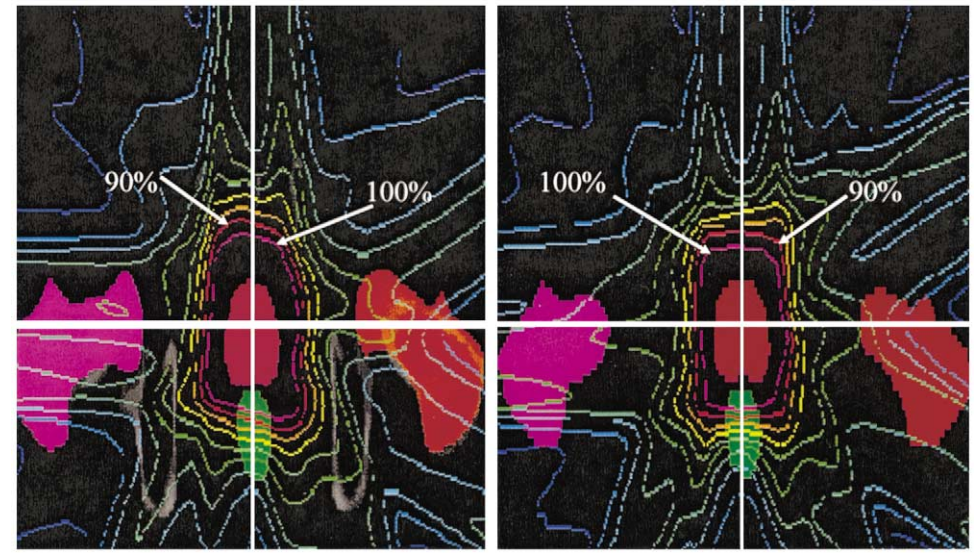

(a)

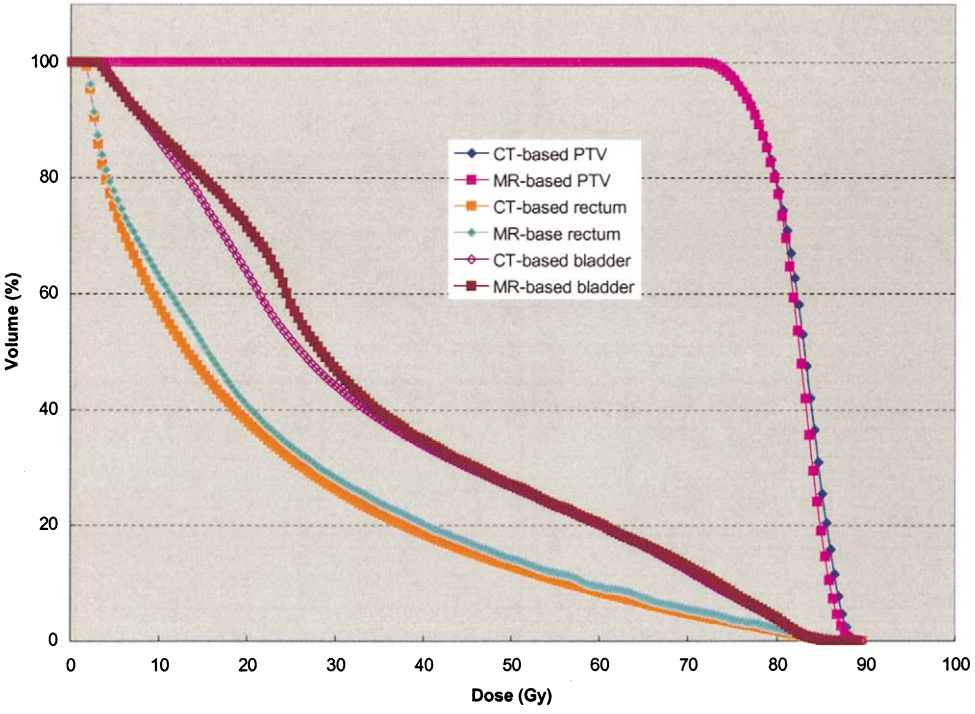

(b)

Fig. 1. Comparison of isodose distributions (a) and dose–volume histograms (b) for planning target volume, rectum, and bladder between computed tomography–based and magnetic resonance imaging–based intensity-modulated radiation therapy plans. The isodose lines are 100%, 90%, 80%, 70%, 60%, 50%, 40%, 30%, 20%, and 10%, respectively.

These differences may have small effects on the DVH comparison between MRI and CT in this work (see the following section). However, this effect will not be a problem when contours are drawn directly on MRI for MRI-based treatment planning in the future.

Comparison of CT- and MR-based treatment plans

Figure 1a shows an example of isodose distributions of IMRT plans based on CT and MRI. The data were taken from Patient 1. It can be seen that the 2 plans look very similar in terms of isodose distributions and they are all

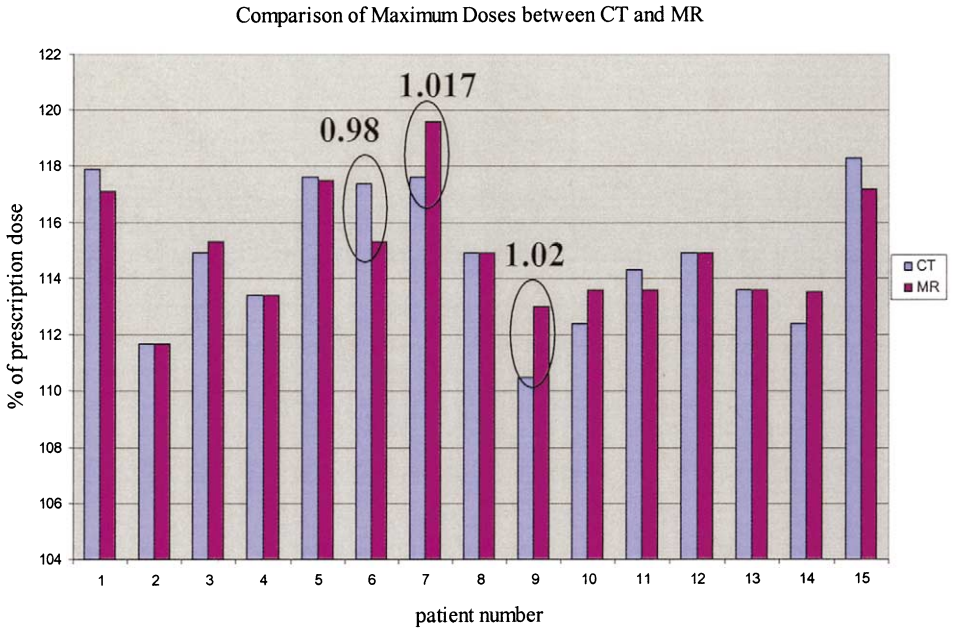

Fig. 2. Comparison of the maximum doses between computed tomography–based and magnetic resonance imaging–based intensity-modulated radiation therapy plans.

acceptable according to our clinical criteria. Figure 1b further compares the DVHs from the CT-based and MRI-based IMRT plans for the same patient. Again the differences are clinically insignificant. The differences for the bladder partially are due to the small differences in the structure volumes between the two image modalities. Because of the voxel size difference between MRI and CT, the bladder volumes may differ by 7% in some cases. As we have mentioned previously, this effect will no longer be a problem when we perform contouring and treatment planning on MRI directly.

Maximum doses

Figure 2 shows the maximum doses between CT- and MRI-based plans. Our clinical criterion for maximum dose

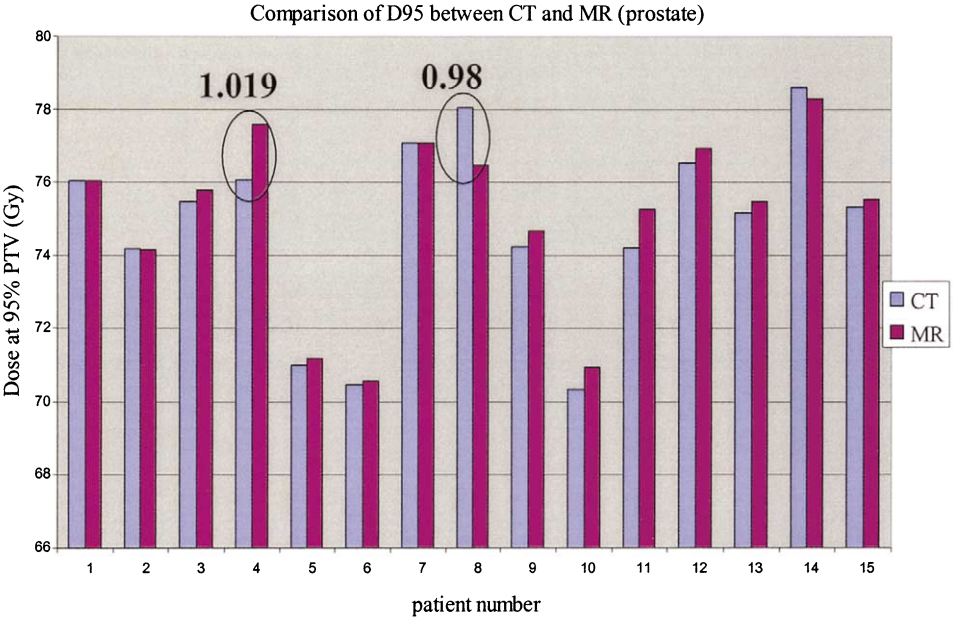

Fig. 3. Comparison of the planning target volume doses between computed tomography–based and magnetic resonance imaging–based intensity-modulated radiation therapy plans.

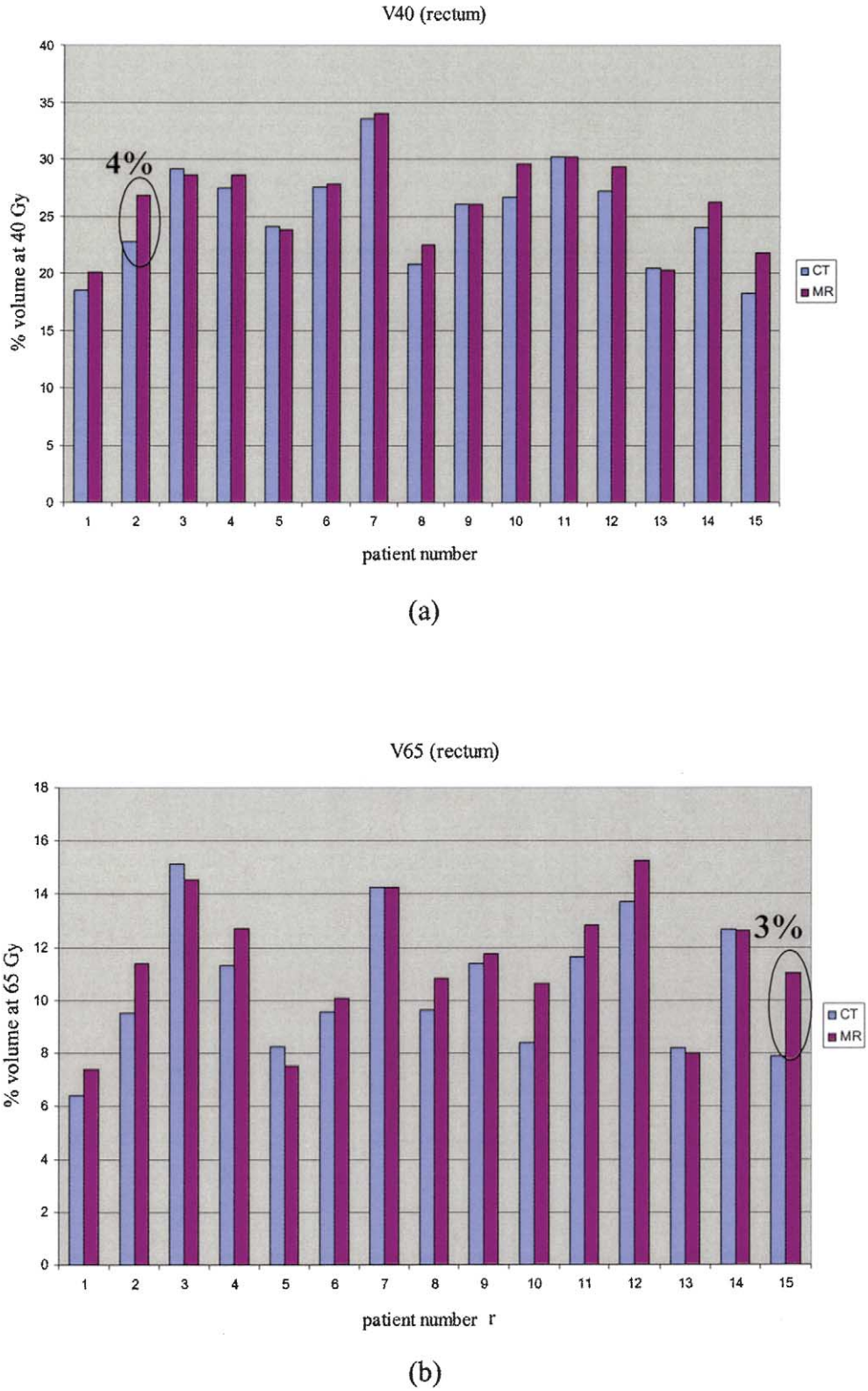

Fig. 4. Comparison of V40 (a) and V65 (b) of the rectum between computed tomography–based and magnetic resonance imaging–based intensity-modulated radiation therapy plans.

is below 120% of the prescription dose. Our results showed that the maximum doses were within 120% for all 15 patients and the dose differences between the CT-based and MRI-based plans were within 2%.

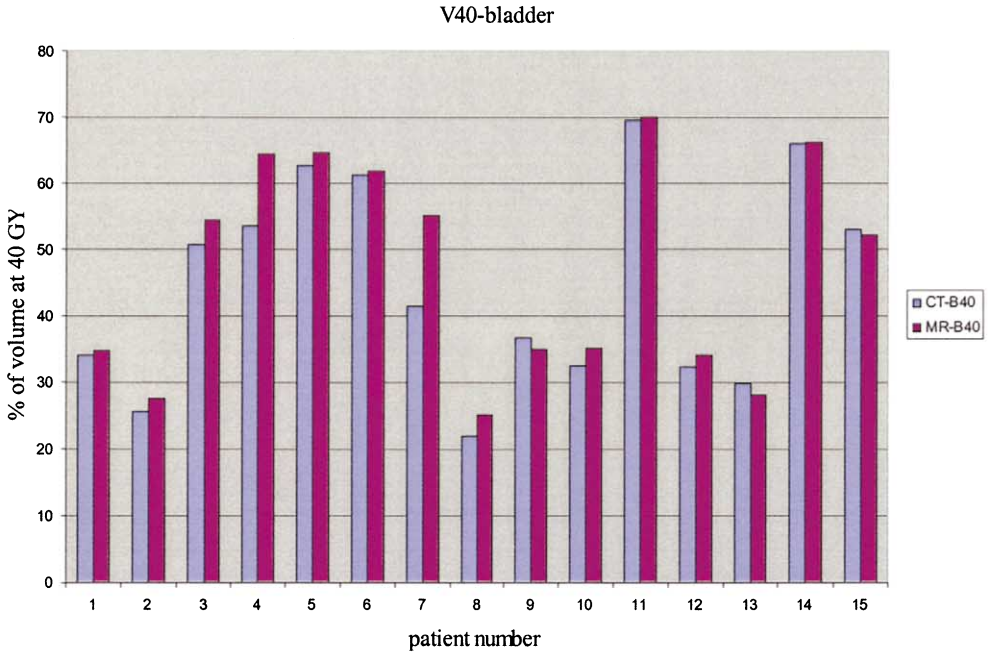

(a)

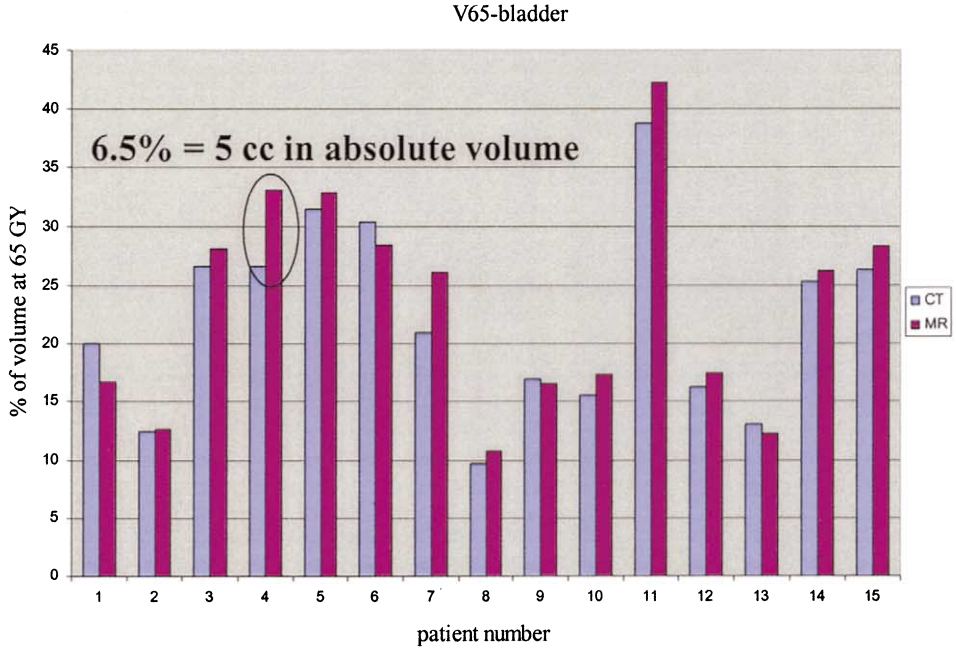

(b)

Fig. 5. Comparison of V40 (a) and V65 (b) of the bladder between computed tomography–based and magnetic resonance imaging–based intensity-modulated radiation therapy plans.

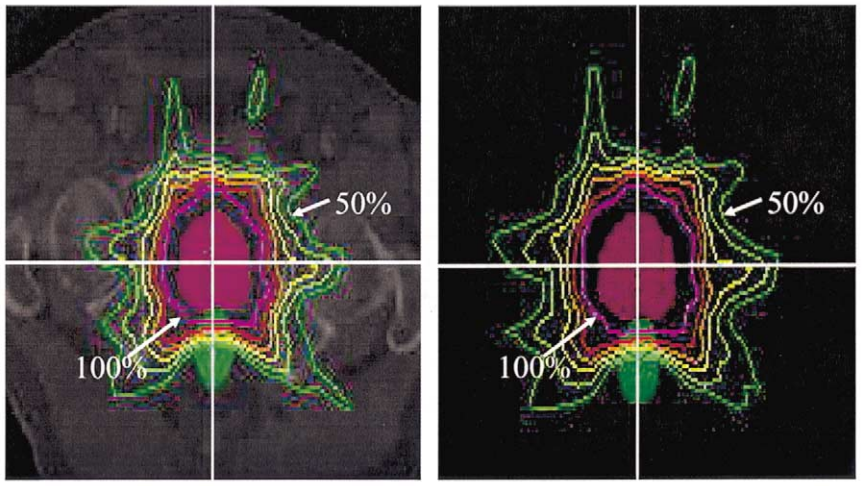

(a)

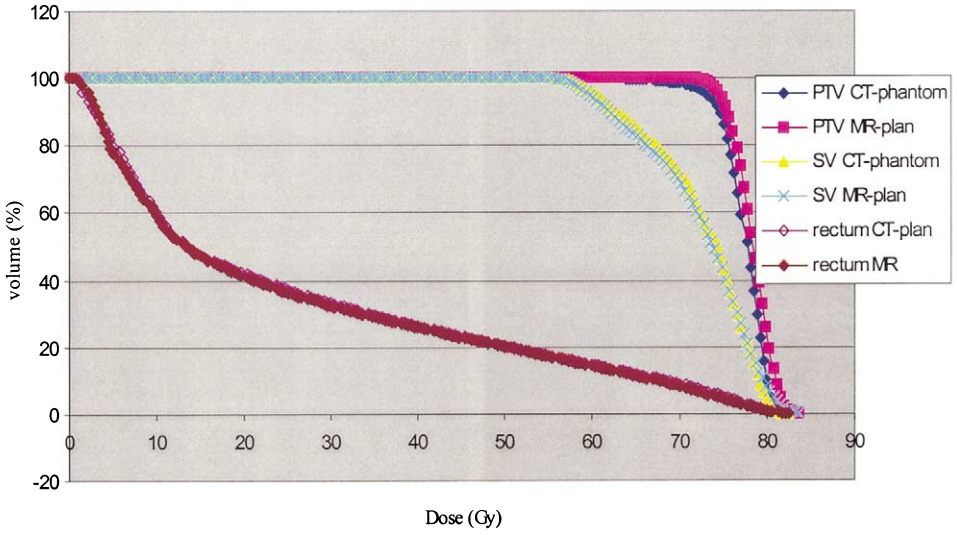

(b)

Fig. 6. Isodose distributions of a magnetic resonance imaging–based treatment plan and the plan recomputed using patient computed tomography data (a) and the corresponding dose–volume histograms for the planning target volume, seminal vesicles, and the rectum (b). The isodose lines are 100%, 90%, 80%, 70%, 60%, and 50%, respectively.

PTV doses

We have compared DVHs for prostate PTV using D95. Figure 3 shows the D95 values from CT-based plans and MRI-based plans for the 15 patients investigated. The largest difference in dose coverage between the two plans was 2% of the prescription dose for Patient 8.

Rectal doses

Figure 4 gives V40 and V65 values for the rectum. As can be seen from Fig. 4a, the largest difference in V40 is 4% (= 3 cc in absolute volume) for Patient 2, whose rectal volumes differed by 4% (3 cc in absolute volume) between CT and MRI as shown in Table 2. The differences in V65 were all within 3% between CT-based and MRI-based plans as seen in Fig. 4b. All the V40 and V65 values meet our clinical acceptance criterion.

Bladder doses

Figure 5 shows the V40 and V65 values for the bladder. Again, the differences between CT-based and MRI-based treatment plans are clinically acceptable. The maximum difference is 6.5% (= 5 cc absolute volume) in V65 for Patient 4 (Fig. 5b), which can be partially attributed to the 3% (2 cc in absolute volume) uncertainty of the contours between CT and MRI.

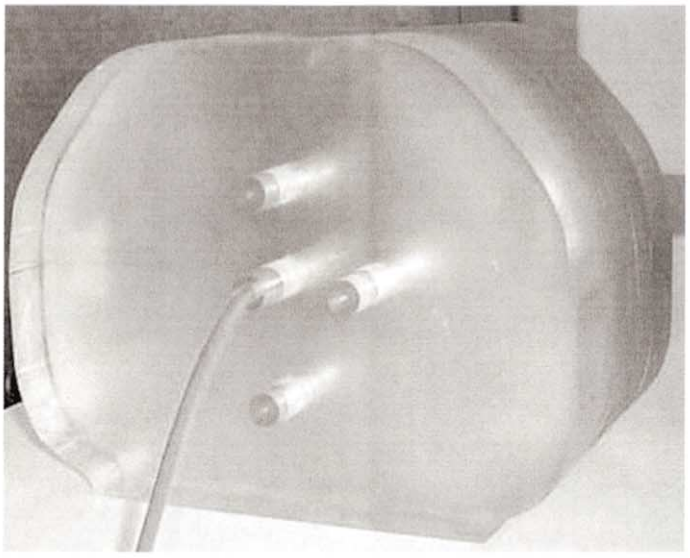

(a)

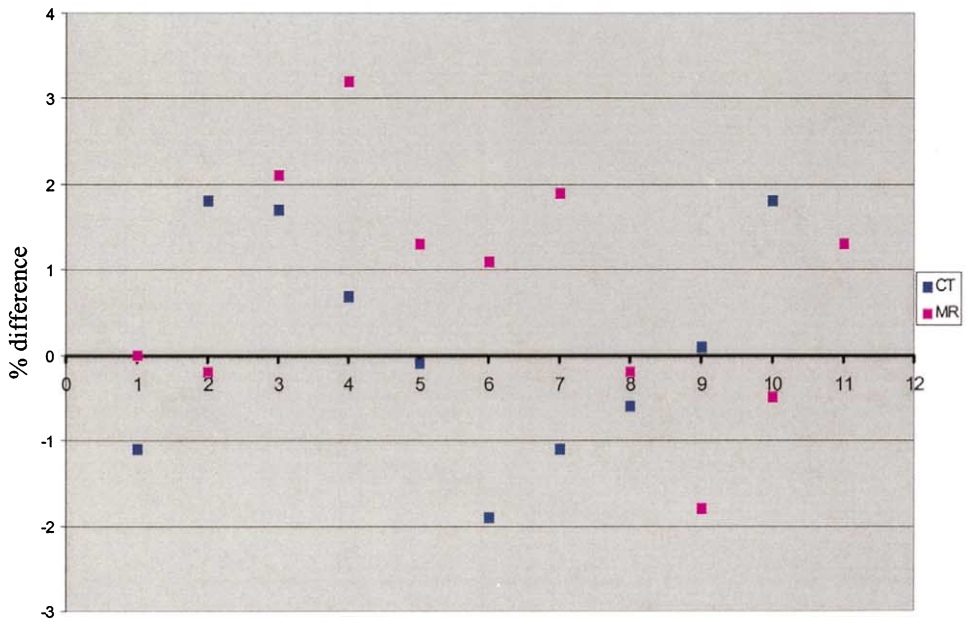

(b)

Fig. 7. An intensity-modulated radiation therapy (IMRT) quality assurance (QA) phantom used for this study (a) and the percent differences in isocenter doses between computed tomography–based and magnetic resonance imaging–based IMRT plans measured using the QA phantom.

Quality assurance for IMRT

To validate the dosimetric accuracy of MRI-based treatment planning, we have recomputed the patient dose distributions using the patient CT data and the MLC leaf sequences generated from the MRI-based patient IMRT plans. Figure 6a shows the isodose distributions of the IMRT plan generated based on MRI data and that recomputed based on CT data, and Fig. 6b shows the DVHs of the PTVs and the rectum for the two plans. The differences in dose are generally smaller than 2% of the prescription dose (or within 2 mm of isodose shift). Small differences in DVH were found because of the differences in structure volumes between CT and MRI. These small differences are considered to be clinically insignificant.

We also performed measurements on a quality assurance (QA) phantom to verify Monitor Unit (MU) calculations for

MRI based treatment planning. Figure 7a shows the QA phantom we used routinely for IMRT dosimetry verification. The hybrid plans were generated for both the CT-based plans and the MRI-based plans using the leaf sequences and associated MU designed for the corresponding patient plans. The physical phantom was irradiated using the same leaf sequences to verify the dosimetric accuracy of the treatment plans. The MRI-based MU calculation is accurate in comparison with measurements as shown in Fig. 7b. The largest difference of 3.2% between MRI-based dose calculation and measurements was seen on Patient 4. Figure 7b also clearly demonstrated that MUs calculated based on MRI and those calculated based on CT are consistent.

DISCUSSION

Effect of MRI distortions on dose calculation

At our institution, we have clinically implemented MRI-based treatment planning for prostate IMRT. To ensure the dosimetry accuracy of MRI-based treatment planning, we selected patients with maximum lateral dimensions $\leq$38 cm. For patient lateral sizes larger than 38 cm we use the CT and MRI fusion technique with CT-based dose calculation. For 6 weeks, we measured lateral dimensions for all the new prostate IMRT patients and found that 41 of 46 (89%) patients were $\leq$38 cm, 4 of 46 (9%) were 39–39.5 cm, and only 1 (2%) patient was greater than 40 cm in lateral dimensions. As shown in Table 1, the GDC software worked well for patient sizes less than 38 cm with residual distortion errors less than 7 mm.

In this study, we have demonstrated that with GDC, MRI-based treatment planning is adequate for prostate IMRT using the Corvus inverse planning system. The residual MRI distortions did not seem to affect IMRT dose calculations, because most differences in the external contours along the major axes were less than 1 cm. The difference could be more than 1 cm in other directions off the major axes and the effect could be greater if a beam was incident in those directions. However, when multiple beams were used in an IMRT treatment, it is unlikely that a treatment plan will be affected significantly if only one or two beams will be affected by 1–2 cm differences in the external contours of the patient.

Our results showed that the difference between CT-based and MRI-based treatment planning for maximum target doses is less than 2%, and for D95 of the prostate is also within 2%. The differences in V40 and V65 for the rectum are within 4%. The largest discrepancies of V40 and V65 for the bladder were seen on Patients 4 and 7, which did not correspond to the largest residual distortions appeared on Patients 1, 5, 6, and 8 with lateral dimensions greater than 40 cm. The dose discrepancies on V40 and V65 of the bladder were believed to be caused by the small volume discrepancies between the two imaging modalities as well as the uncertainties introduced by manually transferring the contours from CT to MRI. However, these differences will no longer be a problem when MRI alone is used for treatment planning.

Creating MR-based DRR for patient setup

Digitally reconstructed radiographs (DRRs) from patient CT data are routinely used for patient initial setup verification by comparing with images taken using portal film or electronic portal imaging devices. However, MRI-derived DRRs do not provide bony structure information and therefore cannot be used directly for checking patient positions. To overcome this problem, relevant bony structures including pubic symphysis, acetabulum, femoral heads and sacrum were contoured using AcQSim and assigned a bulk density of 2.0 g/cm^3. The bony structures were then clearly shown on the MRI-derived DRRs, which could be used for patient initial setup verification by comparing with portal films. The accuracy of this method was verified by comparing with CT-derived DRRs (within 2–4 mm) based on our contour experiences on MRI. The BAT (B-mode Acquisition and Targeting, NOMOS Corp.) ultrasound system is also used for daily target localization to correct for prostate interfraction motion. The BAT ultrasound images agreed better with MRI-generated soft-tissue contours than CT-generated contours.

CONCLUSIONS

This article investigates MRI-based treatment planning for IMRT of prostate cancer. We summarize the results and conclusions of this investigation as follows.

1. We investigated the effect of MRI residual distortion after GDC on IMRT treatment planning and dosimetry accuracy. The residual distortion errors are less than 1 cm and will have negligible clinical impact for more than 90% of the prostate patients whose lateral dimensions are $<$40 cm.
2. We also studied structure volume differences between CT and MRI on the AcQSim and Corvus systems, which led to small discrepancies in DVH curves for those structures with significant differences. These differences reflected the inherent uncertainties of target and structure delineation using different imaging modalities and different treatment planning systems. However, these DVH discrepancies will not be a problem when MRI alone is used for treatment planning because both structure contouring and treatment optimization will be performed using the same imaging modality.
3. We evaluated MRI- and CT-based IMRT treatment optimization for plan consistency. Because both planning techniques will be used clinically and in different treatment protocols, it is essential to ensure IMRT plans using both imaging modalities are consistent in terms of target coverage, dose conformity, and normal tissue sparing. Our results showed that no clinically significant differences were found between MRI- and CT-based treatment plans using the same beam arrangements, dose constraints, and optimization parameters.
4. We validated the dosimetry accuracy of MRI-based treatment planning by recomputing MRI-based IMRT

plans using patient CT data and an IMRT QA phantom. The differences in dose distributions between MRI plans and the corresponding recomputed plans were generally within 3%/3 mm. The differences in isocenter doses between MRI dose calculation and phantom measurements were within our clinical criterion of 4%.

5. To facilitate initial patient setup, MRI-based DRRs were generated, which included structure outlines for relevant bony landmarks such as pubic symphysis, acetabulum, femoral heads, and sacrum. The BAT ultrasound system was used to localize the treatment target for prostate IMRT.

REFERENCES

1. Schellhammer PF, el Mahdi AM, Higgins EM, *et al.* Prostate biopsy after definitive treatment by interstitial 125 iodine implant or external beam radiation therapy. *J Urol* 1987;137: 897–901.
2. Zelefsky MJ, Leibel SA, Gaudin PB, *et al.* Dose escalation with three-dimensional conformal radiation therapy affects the outcome in prostate cancer. *Int J Radiat Oncol Biol Phys* 1998;41:491–500.
3. Hanks GE, Hanlon AL, Schultheiss TE, *et al.* Dose escalation with 3D conformal treatment: Five year outcomes, treatment optimization and future directions. *Int J Radiat Oncol Biol Phys* 1998;41:501–510.
4. Hanks GE. Progress in 3D conformal radiation treatment of prostate cancer. *Acta Oncol* 1999;38(Suppl. 13):69–74.
5. Pollack A, Zagars GK, Rosen II. Prostate cancer treatment with radiotherapy: maturing methods that minimize morbidity. *Semin Oncol* 1999;26:150–161.
6. Pollack A, Zagars GK, Smith LG, *et al.* Preliminary results of a randomized radiotherapy dose-escalation study comparing 70 Gy with 78 Gy for prostate cancer. *Jof Clinical Oncology* 2000;18:3304–3911.
7. Pollack A, Zagars GK, Starkschall G, *et al.* Prostate cancer radiation dose response: Results of the M. D. Anderson phase III randomized trial. *Int J Radiat Oncol Biol Phys* 2002;53: 1097–1105.
8. Yeoh EEK, Fraser RJ, McGowan RE, *et al.* Evidence for efficacy without increased toxicity of hypofractionated radiotherapy for prostate carcinoma: Early results of a Phase III randomized trial. *Int J Radiat Oncol Biol Phys* 2003;55:943–955.
9. Khoo VS, Adams EJ, Saran F, *et al.* A comparison of clinical target volumes determined by CT and MRI for the radiotherapy planning of base of skull meningiomas. *Int J Radiat Oncol Biol Phys* 2000;46:1309–1317.
10. Tanner SF, Finnigan DJ, Khoo VS, *et al.* Radiotherapy planning of the pelvis using distortion corrected MR images: The removal of system distortions. *Phys Med Biol* 2000;45:2117–2132.
11. Potter R, Heil B, Schneider L, *et al.* Sagittal and coronal planes from MRI for treatment planning in tumors of brain, head and neck: MRI assisted simulation. *Radiother Oncol* 1992;23:127–130.
12. Rasch C, Barillot I, Remeijer P, *et al.* Definition of the prostate in CT and MRI: A multi-observer study. *Int J Radiat Oncol Biol Phys* 1999;43:57–66.
13. Krempien RC, Schubert K, Zierhut D, *et al.* Open low-field magnetic resonance imaging in radiation therapy treatment planning. *Int J Radiat Oncol Biol Phys* 2002;53:1350–1360.
14. Debois M, Oyen R, Maes F, *et al.* The contribution of magnetic resonance imaging to the three-dimensional treatment planning of localized prostate cancer. *Int J Radiat Oncol Biol Phys* 1999;45:857–865.
15. Chen L, Price R, Li J, *et al.* Evaluation of MRI-based treatment planning for prostate cancer using the AcQplan system [Abstract]. *Med Phys* 2003;30:1507.
16. Beavis AW, Gibbs P, Dealey RA, *et al.* Radiotherapy treatment planning of brain tumours using MRI alone. *Br J Radiol* 1998;71:544–548.
17. Guo WY. Application of MR in stereotactic radiosurgery. *J Magn Res Imag* 1998;8:415–420.
18. Mah D, Michael S, Hanlon A, *et al.* MRI simulation: Effect of gradient distortions on three-dimensional prostate cancer plans. *Int J Radiat Oncol Biol Phys* 2002;53:757–765.
19. Mah D, Steckner M, Palacio E, *et al.* Characteristics and quality assurance of a dedicated open 0.23 T MRI for radiation therapy simulation. *Med Phys* 2002;29:2541–2547.
20. Michiels J, Bosmans H, Pelgrims P, *et al.* On the problem of geometric distortion in magnetic resonance images for stereotactic neurosurgery. *Magn Res Imag* 1994;12:749–765.
21. Mizowaki T, Nagata Y, Okajima K, *et al.* Reproducibility of geometric distortion in magnetic resonance imaging based on phantom studies. *Radiother & Oncol* 2000;57:237–242.
22. Lee YK, Bollet M, Charles-Edwards G, *et al.* Radiotherapy treatment planning of prostate cancer using magnetic resonance imaging alone. *Radiother & Oncol* 2003;2:203–216.
23. Ma C-M, Mok E, Kapur A, *et al.* Clinical implementation of a Monte Carlo treatment planning system. *Med Phys* 1999;26: 2133–2143.
24. Ma C-M, Pawlicki T, Jiang SB, *et al.* Monte Carlo verification of IMRT dose distributions from a commercial treatment planning optimization system. *Phys Med Biol* 2000;45:2483–2495.
25. Chen L, Li J, Mah D, *et al.* Monte Carlo investigation of dosimetry accuracy for MR-based treatment planning [Abstract]. *Med Phys* 2002;29:1339.
26. Fransson A, Andreo P, Potter R. Aspects of MR image distortions in radiotherapy treatment planning. *Strahlenther Onkol* 2002;177:59–73.
27. Pollack A, Price RA. IMRT for prostate cancer. In: Palta JR, Mackie TR, editors. Intensity-modulated radiation therapy: The state of the art. AAPM Monograph No. 29. WI. Medical Physics Publishing, Madison; 2003. pp. 617–630.